Theoretical approach of freeze seawater desalination on flake ice maker utilizing LNG cold energy

Wensheng Cao [a,c,d], Clive Beggs [b], Iqbal M. Mujtaba [b,*]

[a] College of Mechanical and Energy Engineering, Jimei University, Xiamen 361021, China

[b] School of Engineering and Informatics, University of Bradford, West Yorkshire, Bradford BD7 1DP, UK

[c] Fujian Province Key Lab of Energy Cleaning Utilization and Development, Jimei University, China

[d] Cleaning Combustion and Energy Utilization Research Center of Fujian Province, Jimei University, China

* Corresponding author. E-mail address: I.M.Mujtaba@bradford.ac.uk (Prof. I.M. Mujtaba).

Abstract

In this work, a novel concept in freeze desalination (FD) was introduced. Nowadays the total liquefied natural gas (LNG) production capacity has reached 290 Megatons per year. Its enormous cold energy released from re-gasification can be used in the freeze desalination process to minimize the overall energy consumption. A process of FD on flake ice maker utilizing LNG cold energy was designed and simulated by HYSYS software. An ice bucket on flake ice maker was chosen as seawater crystallizer mainly due to its continuous ice making and removing ice without heat source. A dynamic model of the freezing section has been developed and simulated through gPROMS software. The results show that the consumption of 1 kg equivalent LNG cold energy can obtain about 2 kg of ice melt water. In addition, it is shown that the power consumption of this LNG/FD hybrid process is negligible.

Keywords:

Freeze desalination; Flake ice maker; LNG cold energy; Dynamic modeling; Ice growth

Nomenclature

Symbols

α Heat transfer coefficient, W/m^{2}K

T Temperature, ^{o}C or K

λ Heat conductivity coefficient, W/m K

K Overall heat transfer coefficient, W/m^{2}K

δ Thickness of wall, m

x Thickness of ice layer, m

ρ Density, kg/m^3

L Latent heat of ice, J/kg

C Mass fraction of salt

D Diameter, m

u Velocity, m/s

ν Kinematic viscosity, m^2/s

Pr Prandtl number

Q Heat load of flake ice maker, kW

q Flow rate, m^3/s or kg/s

c Specific heat, J/kg K

h Specific enthalpy, J/kg

s Specific entropy, J/kg K

Subscripts

c coolant or refrigerant

s seawater

w wall

i ice layer

p particle

NG natural gas

LNG liquefied natural gas

1. Introduction

Desalination is an important and effective way to mitigate water-shortages in many arid areas around the world. According to the 24^{th} IDA (International Desalination Association) Worldwide Desalting Plant Inventory [1], the total capacity of completed desalination plants has been reached 71.9×10^6 m^3/d by the end of 2011. It would be more significant to improve the capacity of a plant with higher productivity.

Desalination is an energy-intensive industry that not only depletes fossil fuels, but also results in the emission of greenhouse and other undesirable gases. Driving the process by renewable energies is thus an important development goal, provided that the cost of the water produced can be maintained at an acceptably low level. Thermal desalination processes can be driven by solar or geothermal heat sources, and electrically powered desalination processes have been coupled to wind turbines. However, these renewable energy sources can be problematic, either because the energy density produced is too low for desalination purposes, or because it is

unsteady, not to mention the additional maintenance and infrastructure costs associated with the use of renewable energy sources [2].

Freeze desalination (FD) refers to the process in which fresh water is extracted by harvesting and melting the ice crystals from the chilled feed (seawater or brackish water) [3]. In this process, the saline water is cooled and frozen under controlled conditions. Almost all the salt is rejected by the ice crystals generated and as a result, fresh water can be obtained from the melted ice. Theoretically, only about 1/7 of the energy required to boil a saline solution is needed for the freeze-melt process [4]. In general, the FD process (see Fig. 1) consists of four steps: (a) pre-cooling of the feed brine, (b) crystallization of the ice crystals, (c) separation of the ice crystals from the brine solution and (d) washing and melting ice crystals to obtain high purity water.

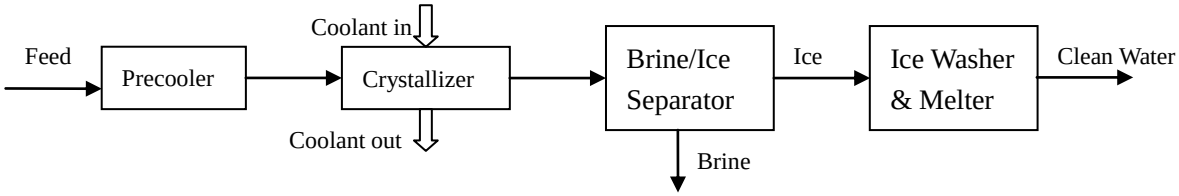

Fig. 1 Diagram of indirect contact freeze desalination (ICFD).

While FD has potential, its adoption as a desalination technology has so far been very limited [3]. One reason for this is the ready availability of convenient fossil fuels, such as natural gas (NG), in countries that rely heavily on desalination, with the result that thermal desalination technologies tend to be favored. However, rather surprisingly, NG production also has the potential to facilitate the use of FD. This is because considerable amounts of waste ‘cold’ energy are released during the re-gasification process by which LNG is turned into NG. The cold energy refers to the heat absorption effect from the ambient environment that occurs when LNG is re-gasified at the LNG terminals. LNG occupies only a fraction (1/600) of the volume of NG, making it much easier to handle and transport, with the NG stored in a liquid form at atmospheric pressure at about 110 K. Hence, LNG must be re-gasified before being utilized in its gaseous form, a process that absorbs about 837 KJ/Kg LNG from the surroundings [5]. Owing to the low temperature, high energy density and blooming global LNG market, LNG cold energy is now recognized as a high quality energy source with which to cool media [4].

At present, there are 58 sets of large-scale base load LNG projects built in the world, with the total LNG production capacity estimated to be 290 Megatons per year [6, 23]. The growth in LNG production capacity between 1964 and 2012 is illustrated in Fig. 2.

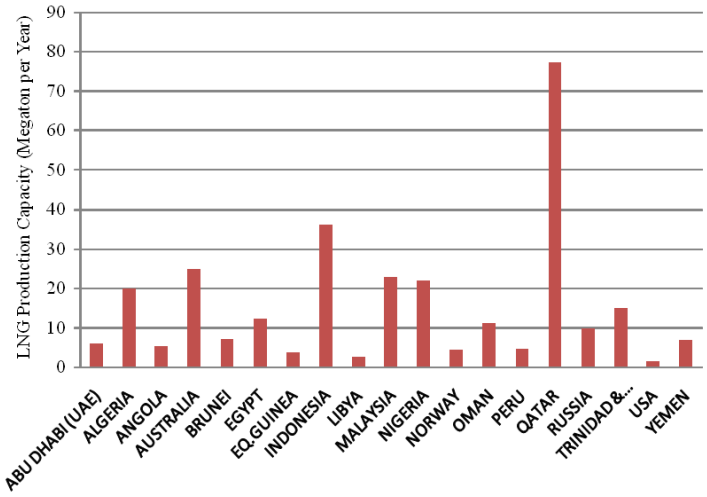

Fig. 2 LNG production capacity of built LNG projects (1964-2012) [6, 23]

Fig. 3 shows a prospect of LNG production capacity of new-built and proposed LNG projects between 2013 and 2019. By 2019, America will become the largest producer and exporter of LNG, overtaking Qatar currently ranked no. 1.

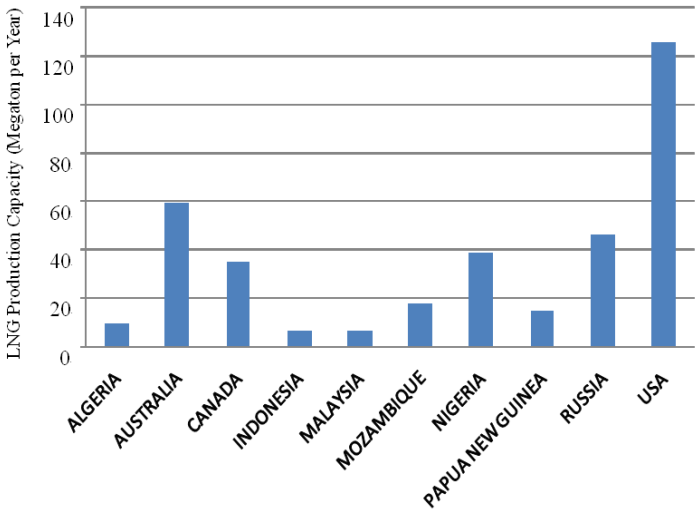

Fig. 3 LNG production capacity of new-built and proposed LNG projects (2013-2019 onshore) [6, 23]

Considering the characteristic and mechanism of FD process, this system requires large quantities of high quality cold energy. For the FD process, cold energy is needed to cool and crystallize the pre-cooled saline feed solution. The large amount of cold energy from re-gasification of LNG just happens to meet the energy requirement of FD process – thereby minimizing the overall energy consumption.

Although much researched, the optimum technique for freezing and harvesting ice during FD is not known. Over the years researchers have investigated a variety of techniques. Chen et al. [7] developed two models of ice growth velocity in aqueous solutions derived from an irreversible thermodynamics analysis and the conventional

heat and mass transfer theory, debating with Ratkje and Flesland [8] on modelling the freeze concentration process by irreversible thermodynamics. Shirai et al. [9] investigated the effect of seed ice on formation of tube ice with high purity for a freeze wastewater treatment system with a bubble-flow circulator. Chen et al. [10] experimentally studied the spatial uniformity of solute inclusion in ice formed from falling film flows on a sub-cooled surface. Wakisaka et al. [11] experimentally explored the ice crystallization in a pilot-scale freeze wastewater treatment system. Qin et al. [12] studied the growth kinetics of ice in films spreading along a sub-cooled solid surface. Zhao et al. [13] optimized the ice making period for ice storage system with flake ice maker. Rice and Chau [14] discussed freeze desalination using hydraulic refrigerant compressors. Williams et al. [15] assessed an ice maker machine for desalting brines. Attia [16] proposed a new system for freeze water desalination using auto reversed R-22 vapor compression heat pump. Rane and Padiya [17] studied heat pump operated freeze concentration system with tubular heat exchanger for seawater desalination. Fujioka et al. [18] modeled and applied a progressive freeze-concentration for desalination.

In this study, a new concept was introduced and the use of LNG cold energy coupled with a freeze-melt process to desalinate seawater was investigated, and a dynamic model to evaluate its potential as a desalination technology was also presented.

2. Flake ice maker

In the present study a system was considered, which utilized a flake ice maker, in which a rotary ice blade is used to scrape an ice layer off the sub-cooled surface of a cylindrical heat exchanger. Such machines tend to exhibit higher heat transfer efficiencies compared with other methodologies, such as the tube ice makers. They are also relatively simple and easy to operate. In particular, because the flake ice maker utilizes a mechanical method to remove ice instead of hot gas defrosting, there is no requirement for an additional heat source.

Flake ice makers (Figure 4) produce irregular flake ice with approximate size 40mm×40mm and thickness range from 1.0mm to 2.5mm. They are widely used in industry for controlling chemical reactions and concrete temperature cooling due to the large contact area employed. They are also widely employed to produce ice from seawater to cool and preserve fish. With respect to this, seawater machines differ from the common flake ice makers, insomuch that all the parts employed are

anti-corrosive, with the compressor powerful enough to cool seawater to about -25 ^{o}C.

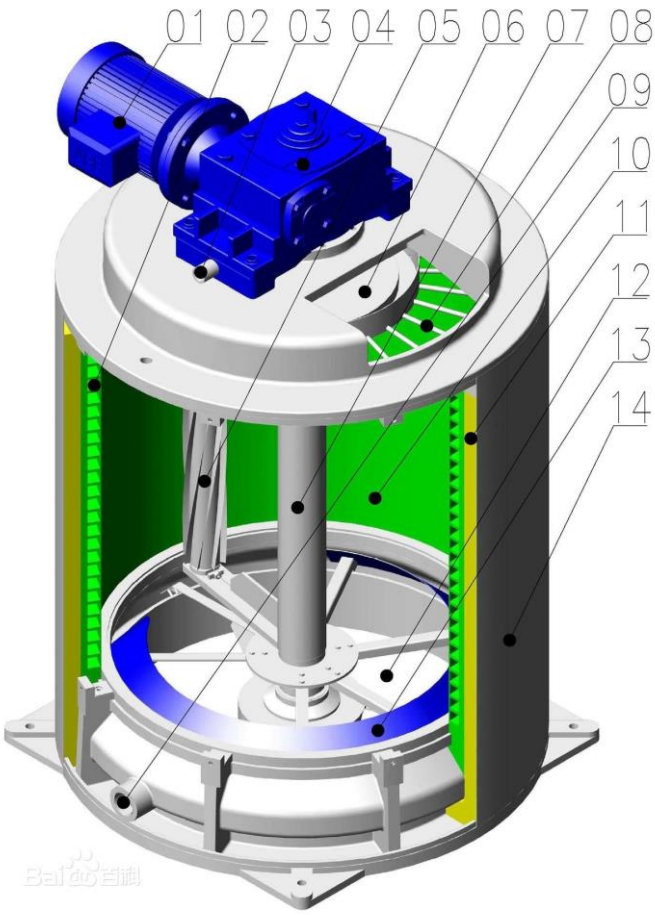

01-Motor, 02-Spiral evaporation pipelines, 03-Seawater supply inlet, 04-Reducer
05-Ice blade, 06-Water distribution pan, 07-Main shaft, 08-Water distribution tubes
09-Exit of water collection dish, 10-Inner wall of evaporator, 11-Insulation material
12-Ice storage bin, 13-Ice drop opening, 14-Outer shell

Fig. 4 Schematic diagram of ice bucket on flake ice maker

The ice flake machine comprises a cylindrical evaporator, on which the ice forms. Seawater is trickled over the inner surface of this evaporator, where it is rapidly cooled to form ice and at the same time the salt ion is excluded from the ice crystal interface. The seawater is fed into a header tank above the evaporator, from which it is evenly sprinkled onto the inner wall of the evaporator through a series of distribution tubes. Any salty water not frozen is allowed to fall into a collection dish, from which it is thrown away. As shown in Figure 4, the ice is harvested by a rotating blade which cuts through the ice layer on the inner wall of the evaporator, dislodging evenly-shaped ice flakes, which fall from the walls and pass out of the ice

drop opening at the bottom of the machine.

3. Utilization of LNG cold energy

The FD process utilizing LNG cold energy is illustrated in Figure 5, which shows the relative arrangement of the refrigerant pump, the ice making evaporator, and the LNG exchanger. In the system the refrigerant is condensed in the LNG heat exchanger, which performs a similar role to the expansion valve in a conventional refrigerant system. Saturated LNG liquid enters the LNG exchanger, where it evaporates to form gaseous NG, a process which involves absorbing heat from the gaseous refrigerant stream (2), which condenses to form liquid refrigerant (3). The liquid refrigerant is then pumped to evaporator where it once again become gaseous, absorbing latent heat from the seawater, which freezes to form ice.

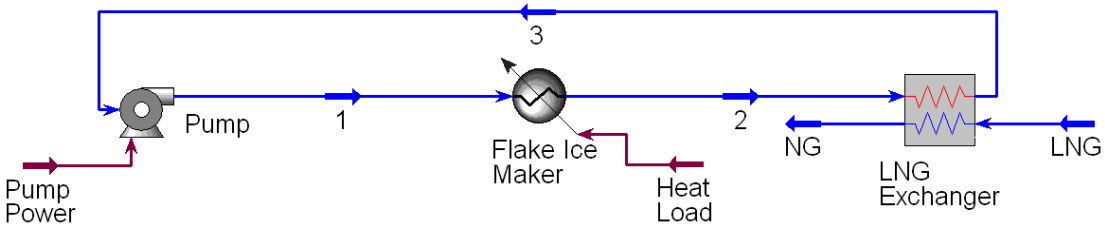

Fig. 5 Process of FD on flake ice maker utilizing LNG cold energy

With the rapid rate at which heat is transferred in the LNG heat exchanger, there is danger that solidification of the refrigerant might occur. Consequently, it would be necessary to employ a refrigerant, with a low operating temperature, such as R410A, which is an environment-friendly, azeotropic mixture (50%/50%) of the refrigerants HFC-32 and HFC-125, and which has a freezing point of -155 ^{o}C.

3.1 Simulation methodology

The simulating calculations and system optimization was carried out using PR-Twu equation of state through HYSYS software [5]. PR-Twu equation is one of the most important Fluid Packages utilized by HYSYS.

The simulation assumed that the freshwater flow was 150 L/h (daily output 3600 kg ice), and that the nominal evaporation temperature was -25 ^{o}C (see Table 1 bold italic). Considering the wash water (accounts for 10% of produced ice) and the concentration of seawater (usually taken as 2 times), the ice maker should produce 167 kg/h ice [$167kg/h\times(100\%-10\%)=150kg/h$, equivalent to 150 L/h freshwater] so the seawater input rate was $167\times2=334L/h$, and the heat load Q of flake ice maker was deduced by

$$Q=q_s c_s \Delta T_s + q_i L \qquad (1)$$

where q_s and q_i are the flow rate of seawater and produced ice respectively (viz. 334L/h, 167kg/h), c_s is the specific heat capacity of seawater (4017J/kg K), ΔT_s is the temperature drop of seawater cooling, and L is the latent heat of ice (334700 J/kg). After the precooling of the ice melting tank, the seawater temperature of the supply inlet (Figure 4 - 03) was set to 2 ^{o}C, so $\Delta T_s = 4$ ^{o}C due to the seawater freezing point was -2 ^{o}C.

By using the above data, Q can be calculated and equals 17 kW.

3.2 Results by HYSYS

The process parameters including mole fraction of components are presented in tables 1 and 2. The pump power was only 5.594×10^{-3} kW, which is the main energy consumption associated with the LNG/FD process.

The following equations show about 2 kg ice melt water can be obtained at the cost of 1 kg equivalent of LNG cold energy.

$$\frac{150kg/h}{78.99kg/h} = 1.9 \sim \frac{167kg/h}{78.99kg/h} = 2.1$$

where 150kg/h is the freshwater mass flow, 167kg/h is produced ice production, and 78.99kg/h is the LNG mass flow (see Table 1 bold italic). The key simulation results were summarized in table 3.

Table 1 Process parameters

Node No.	Temperature (^{o}C)	Pressure (kPa)	Molar Enthalpy (J/mol)	Molar Entropy (J/mol ^{o}C)	Mass Flow (kg/h)	Vapour Fraction
1	-27.85	382.3	-6.69e+5	73.92	242.2	0
2	***-25.00***	332.3	-6.51e+5	147.9	242.2	1
3	-27.46	302.3	-6.69e+5	74.10	242.2	0
LNG	-160.00	120.4	-9.02e+4	77.16	***78.99***	0
NG	-30.00	90.43	-7.73e+4	178.4	78.99	1

Table 3 Simulation results

Freshwater	Ice	LNG: Ice melt water	Pump power
150 kg/h	167 kg/h	1 kg:2 kg	5.594×10^{-3} kW

The matching of the curves between cold composite (LNG stream) and hot composite (refrigerant stream) can be seen from the result shown in Figure 6. The temperature difference between them is very large while LNG is in the two-phase flow state. However, it narrows greatly with the rise in temperature of NG, once the phase-change is complete. This change in temperature difference, accompanied by the reduction in heat transfer, contributes to the energy loss in the heat exchanger.

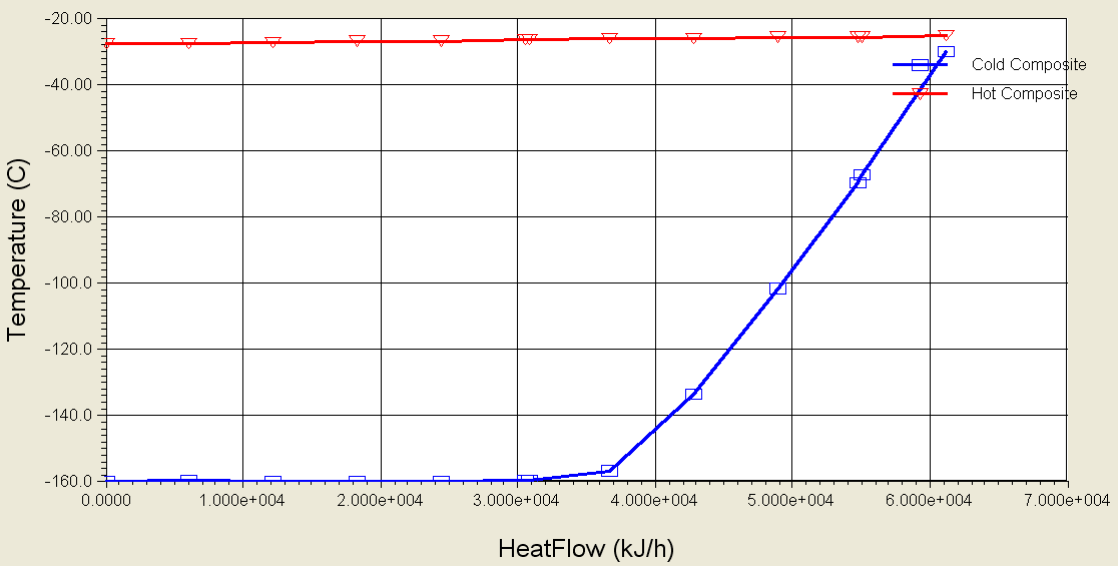

Fig. 6 Heat flow variation as a function of temperature in the pipelines of the LNG exchanger

The heat transfer rate at the evaporator is shown in Fig. 7.

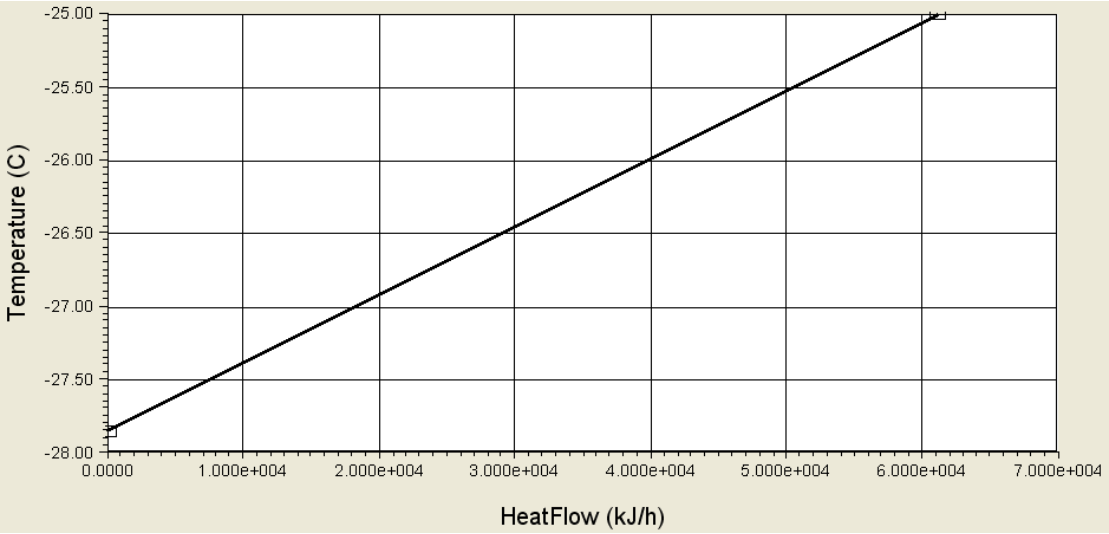

Fig. 7 Heat flow vs. temperature in the spiral evaporation pipelines of the flake ice maker

According to the exergy losses equation (2) and the exergy efficiency equation (3) of the LNG heat exchanger

$$E_{loss} = T_0[q_{LNG}(s_{NG} - s_{LNG}) - q_2(s_2 - s_3)] \qquad (2)$$

$$\eta = \frac{q_2(h_2 - h_3) - q_2 T_0 (s_2 - s_3)}{q_{LNG}(h_{NG} - h_{LNG}) - q_{LNG} T_0 (s_{NG} - s_{LNG})} \times 100\% \qquad (3)$$

where T_0 is the ambient temperature, h is specific enthalpy and s is specific entropy, the exergy analysis results of the LNG Exchanger were: 17.65kW of exergy losses and 8.9% of exergy efficiency.

4. Dynamic model of freezing section

A schematic diagram of the freezing section is shown in Fig. 8.

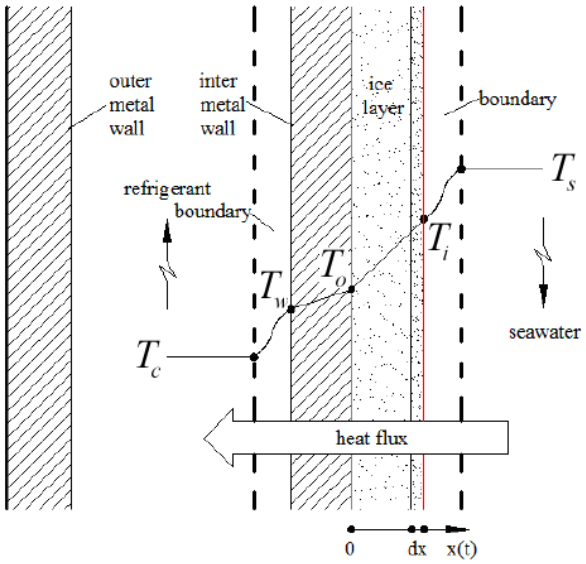

Fig. 8 Schematic diagram of heat transfer on a sub-cooled surface of the ice bucket [19]

The freezing process is characterized by a phase-change heat transfer process during a period of ice making. It can be considered as a one-dimension freezing process. In this heat transfer model, there is a migrating interface between solid phase and liquid phase during the whole process, and the latent heat of phase-change is released at this interface (red line). The phase-change process begins from $x = 0$, then the interface migrates along x axis and its position is a function of time $x(t)$.

The dynamic mathematical model was developed by applying conservation laws of mass and heat to the various phases and components of the freezing section. However, in order to simplify the solution of the equations it is necessary to make the following assumptions concerning the nature of the process:

(a) The compositions and temperatures of the liquid streams at the same height were considered to be the same as the composition C_s and temperature T_s of the bulk liquid in the freezing section.

(b) Variations in density, specific heat, latent heat, heat conductivity coefficient

and heat transfer coefficient, were considered to be negligible over the temperature range of interest.

(c) Crystal size may be defined by a single dimension and, for the purpose of determining crystal mass, crystals are assumed to be spherical.

The heat transfer coefficient of the refrigerant side was given under the condition of forced flow [20] in the pipeline

$$\alpha_c = 0.023 \frac{\lambda_c}{d} \left(\frac{u_c d}{\nu_c} \right)^{0.8} \mathrm{Pr}_c^{0.4} \qquad (4)$$

where d is the feature size of the refrigerant channel and λ_c, u_c, ν_c and Pr_c are the heat conductivity coefficient, velocity, kinematic viscosity and Prandtl number of the refrigerant, respectively.

Falling film flows on a sub-cooled surface can be regarded as the mode of the fluid of constant physical properties over the constant wall temperature plate [20]. So the overall heat transfer coefficient on the seawater side was determined by:

$$\alpha_s = 0.664 \frac{\lambda_s}{h} \left(\frac{u_s h}{\nu_s} \right)^{0.5} \mathrm{Pr}_s^{\frac{1}{3}} \qquad (5)$$

where h is the feature size of the ice bucket and λ_s, u_s, ν_s and Pr_s are the heat conductivity coefficient, velocity, kinematic viscosity and Prandtl number of the seawater, respectively.

The overall heat transfer coefficient of the whole process is determined by four parts, consisting of the refrigerant side, the wall, the ice layer and the seawater side.

$$K = \frac{1}{\frac{1}{\alpha_c} + \frac{\delta}{\lambda_w} + \frac{x}{\lambda_i} + \frac{1}{\alpha_s}} \qquad (6)$$

where δ and x are the thickness of wall and ice layer respectively, λ_w and λ_i are the heat conductivity coefficient of wall and ice layer respectively.

In order to simulate the change in ice thickness with time, according to the law of conservation of energy, the relationship between the four parts of thermal resistance can be changed to

$$\frac{T_i - T_o}{\frac{x}{\lambda_i}} = \frac{T_i - T_c}{\frac{1}{\alpha_c} + \frac{\delta}{\lambda_w} + \frac{x}{\lambda_i}} \qquad (7)$$

where T_i is the temperature of the migrating phase-change interface, T_o is the wall temperature, and T_c is the refrigerant temperature.

During the time of *dt*, the ice layer grows the thickness of *dx*. The analysis of heat transfer rate in this dx ice layer is expressed

$$\frac{T_i - T_o}{\frac{x}{\lambda_i}} dt = \frac{T_i - T_c}{\frac{1}{\alpha_c} + \frac{\delta}{\lambda_w} + \frac{x}{\lambda_i}} dt = \rho_s L dx + \alpha_s \left(T_s - T_i\right) dt \qquad (8)$$

where ρ_s is the density of seawater, L is the latent heat of phase change (ice), and T_s is the bulk temperature of seawater.

The ice growth rate was calculated as

$$v_i = \frac{dx}{dt} = \frac{\frac{T_i - T_c}{\frac{1}{\alpha_c} + \frac{\delta}{\lambda_w} + \frac{x}{\lambda_i}} - \alpha_s \left(T_s - T_i\right)}{\rho_s L} \qquad (9)$$

Crystal growth was calculated from a thermal driving force relationship [21] obtained from a dynamic heat balance on the solid phase. This determined the rate of change of diameter D_p of a single crystal with respect to the difference between the temperature T_i of the ice/liquid interface and temperature T_s of the bulk liquid, according to

$$\frac{dD_p}{dt} = \frac{G}{D_p}\left(T_i - T_s\right) \qquad (10)$$

where *G* is a rate constant defined in terms of a driving force ratio *E* as

$$G = 6.129 \times 10^{-9} E \qquad (11)$$

and *E* is dependent on salt concentration C_s of the bulk liquid according to

$$E = \frac{1}{1 + \frac{77 C_s}{1 - C_s}} \qquad (12)$$

The ice/liquid interface temperature T_i is defined in terms of the freezing temperature of seawater used (271.7K).

The nucleation rate is given as follows

$$Nu = \frac{R_g T_s}{P} \exp\left(\frac{B T_i^2}{T_s \left(T_i - T_s\right)^2} \right) \qquad (13)$$

where R_g is the ideal gas constant, P is Planck's constant and B is an empirical constant which may be calculated by assuming that $Nu = 1$ at nucleation.

5. Discussion and results by gPROMS

Equations (4) to (13) define a set of differential and algebraic relationships which may be employed for simulating the freezing section of the flake ice maker. gPROMS model builder software [22] was used for model development and simulation. Data for the mathematical model have been obtained from the constructional dimensions of the pilot plant flake ice maker [19] and physical properties of brine and ice. These data are presented in Table 4, including the feed boundary inputs and the initial conditions for the start of a simulation experiment. The freezing section is considered to contain an initial falling film on a sub-cooled surface at feed temperature, void of ice, and surrounded by the spiral evaporation pipelines where the refrigerant is fed through in order to start the freezing process and subsequent ice crystal formation.

Table 4 Data used in dynamic modeling

α_c	Heat transfer coefficient of refrigerant side at T_c	1151 W/m^{2}K
T_c	*Feature temperature* of refrigerant	-26.5 ^{o}C
α_s	Heat transfer coefficient of seawater side at T_s	612 W/m^{2}K
T_s	*Feature temperature* of seawater	0 ^{o}C
λ_w	Heat conductivity coefficient of wall Q235	45 W/m K
δ	Thickness of wall	6×10^{-3} m
λ_i	Heat conductivity coefficient of ice layer	2.33 W/m K
ρ_s	Density of seawater	1025 kg/m^3
L	Latent heat of ice	334700 J/kg
R_g	Ideal gas constant	8.314 J/K mol
P	Planck's constant	6.6256×10^{-34} J/s

B	Nucleation rate equation empirical constant	-8.88
	Boundary inputs	
$T_{s.in}$	Inlet temperature of brine	2 ^{o}C
C_s	Mass fraction of salt in brine feed	0.035
	Initial conditions	
x	Thickness of ice layer	0.00 m
D_p	Crystal mean diameter	0.00 m

Figure 9 shows the calculated variation of the thickness of the ice layer as the falling film flows and is cooled to freezing point. It can be seen that although the thickness of the ice increases with time, its growth rate reduces exponentially (Figure 10). This is due to the fact that the thermal resistance to heat transfer increases with ice thickness, causing the heat exchange efficiency to be reduced and the crystallization speed to slow. How the ice growth rate and the overall heat transfer coefficient changes with time are shown in figures 10 and 11. These show a rapid fall in the first 180 seconds followed by a gradual fall. This suggests that in order to optimize the performance of the ice maker, it is important to harvest the ice before it becomes too thick, something that perhaps explains why in the actual process, the ice bucket scraper scrapes ice once every 48 seconds, limiting the ice thickness to a maximum of 3mm. The reporting time interval of data points is 30 seconds, similarly hereinafter.

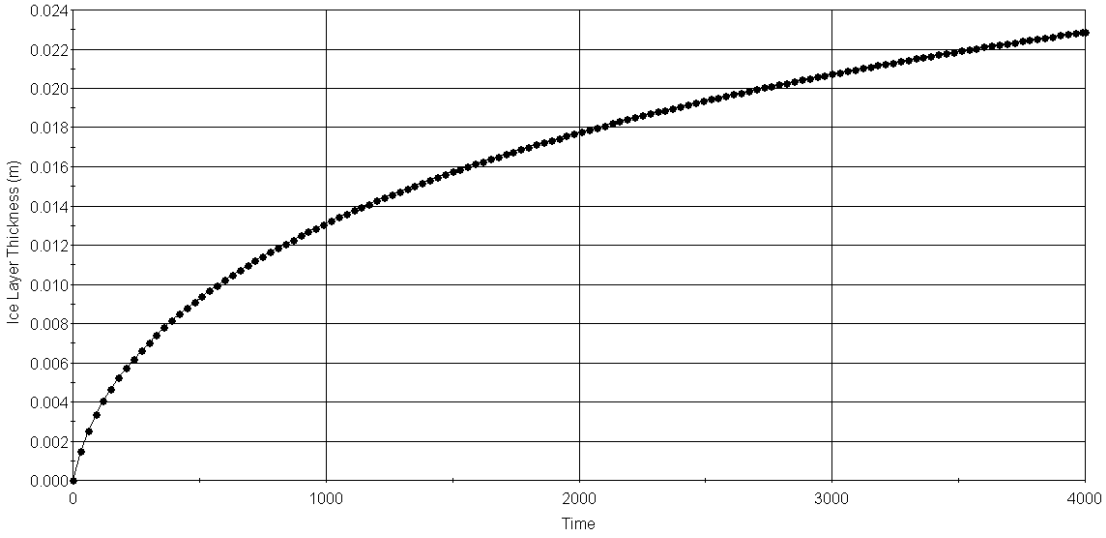

Fig. 9 Variation of the ice layer thickness with time

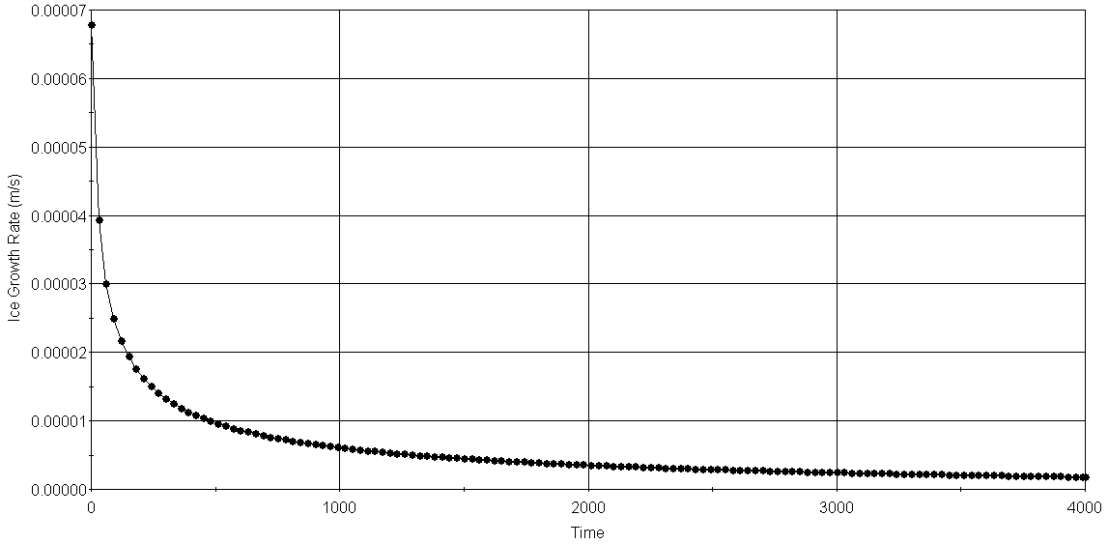

Fig. 10 Variation of the ice growth rate with time

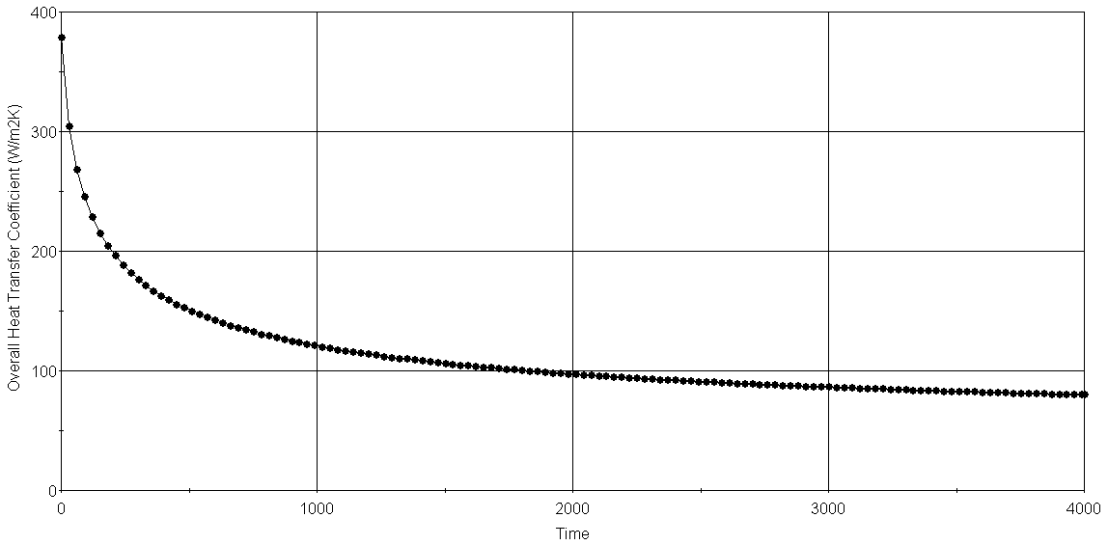

Fig. 11 Variation of the overall heat transfer coefficient of the whole process with time

The relationship between ice growth rate and ice layer thickness is shown in Figure 12, as well as that of the overall heat transfer coefficient vs. ice layer thickness (Figure 13). Careful comparison between these two graphs reveals that the ice growth rate decreases more rapidly with increased ice thickness, compared with the overall heat transfer coefficient.

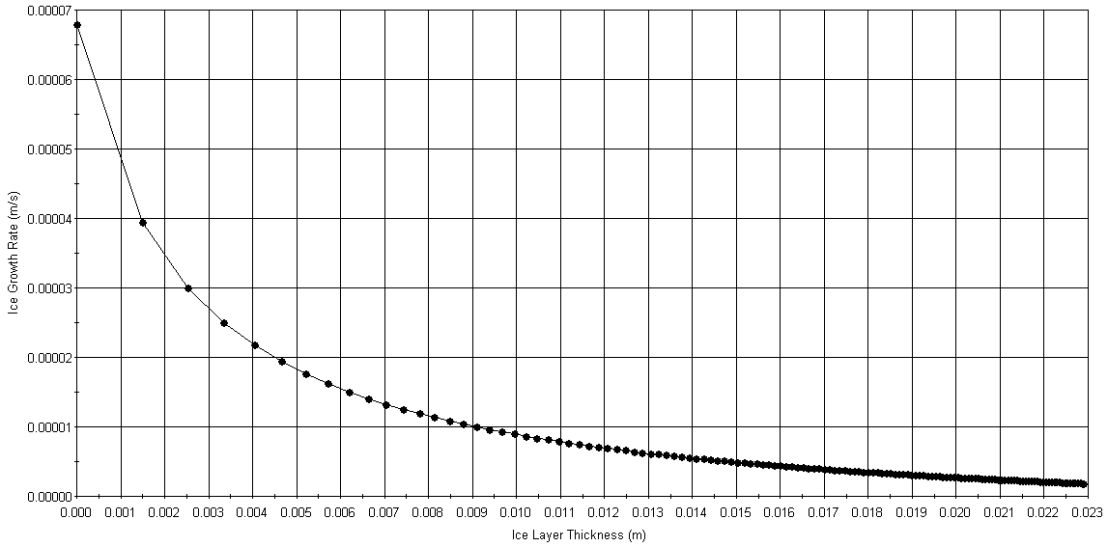

Fig. 12 Ice Growth Rate (m/s) vs. Ice Layer Thickness (m)

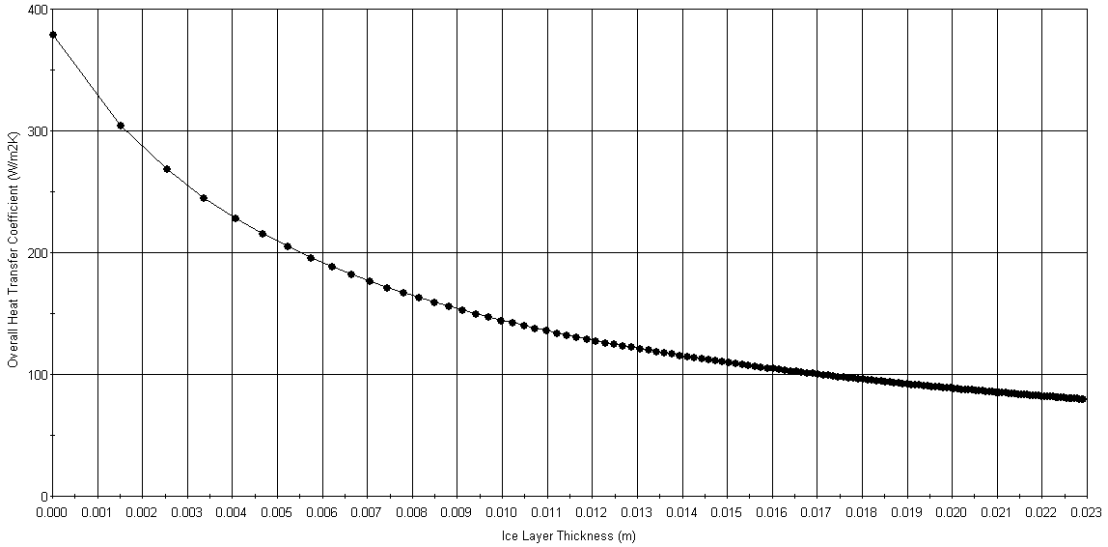

Fig. 13 Overall Heat Transfer Coefficient (W/m2K) vs. Ice Layer Thickness (m)

Our analysis also revealed that the variation of the ice layer thickness with time was dependent on refrigerant temperature (Figure 14), with the rate of ice deposition decreasing as the temperature of the refrigerant increases. When T_c = -32.5 ^{o}C, the growth rate of the ice layer was the greatest, whereas when T_c = -17.5 ^{o}C was considerably slower.

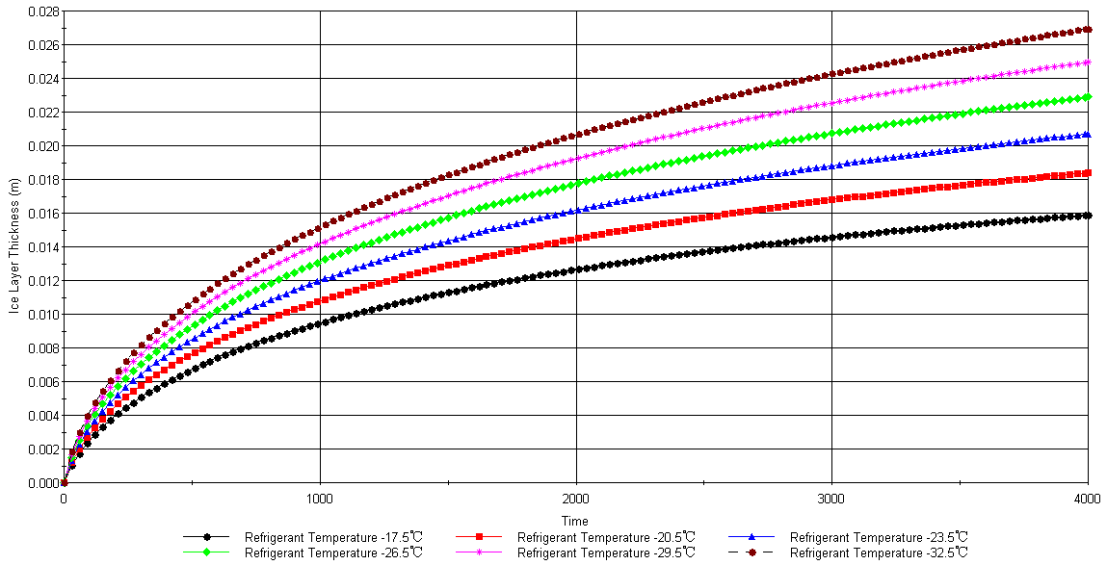

Fig. 14 Variation of the ice layer thickness versus time at different refrigerant temperatures

From the experimental data of seawater desalination on a flake ice maker in [19] shown in Figure 15, it is clear that the higher the refrigerant temperature is, the lower the specific gravity of ice-melt water will be. This suggests that the greater heat transfer rate associated with a lower refrigerant evaporating temperature, might not be beneficial when it comes to the desalination of seawater. If the evaporator temperature is too low, then faster crystallization will occur, resulting in more salt becoming trapped in the ice. By comparison, when crystallization occurs at a slower rate, the exudates become more saline and the ice purer.

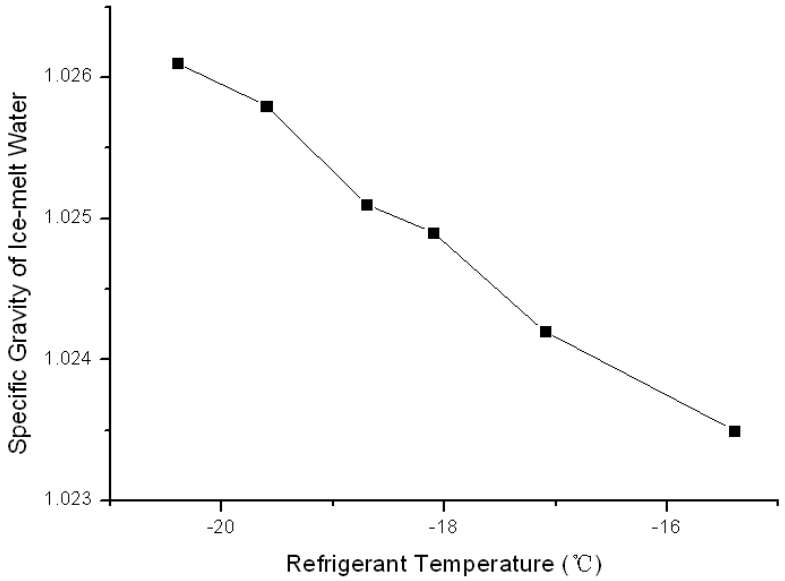

Fig. 15 Effect of refrigerant temperature on specific gravity of ice-melt water [19]

In Fig. 16, the variation of the ice layer thickness with time at different seawater temperatures is presented. From this it can be seen that the growth speed of ice layer

increases with the fall of the temperature of the seawater. When T_s = -1 ^{o}C, the growth speed of ice layer is the fastest, and when T_s = 4 ^{o}C, the slowest. In the operating practice of flake ice maker, when the temperature of the seawater is higher than 2 ^{o}C, the ice layer can grow hardly.

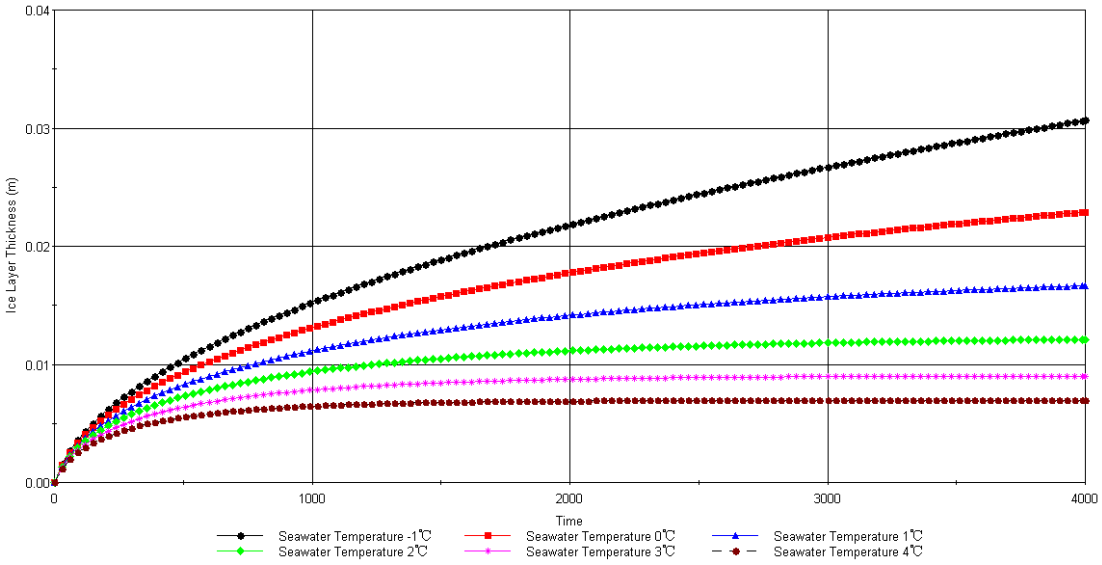

Fig. 16 Variation of the ice layer thickness versus time at different seawater temperatures

As soon as nucleation occurs, crystals start to form as shown in Fig. 17, which illustrates the variation of crystal particle diameter versus time for different mass fractions of salt in seawater feed. From this it is clear that crystal particles grow faster when the seawater contains low concentrations of salt.

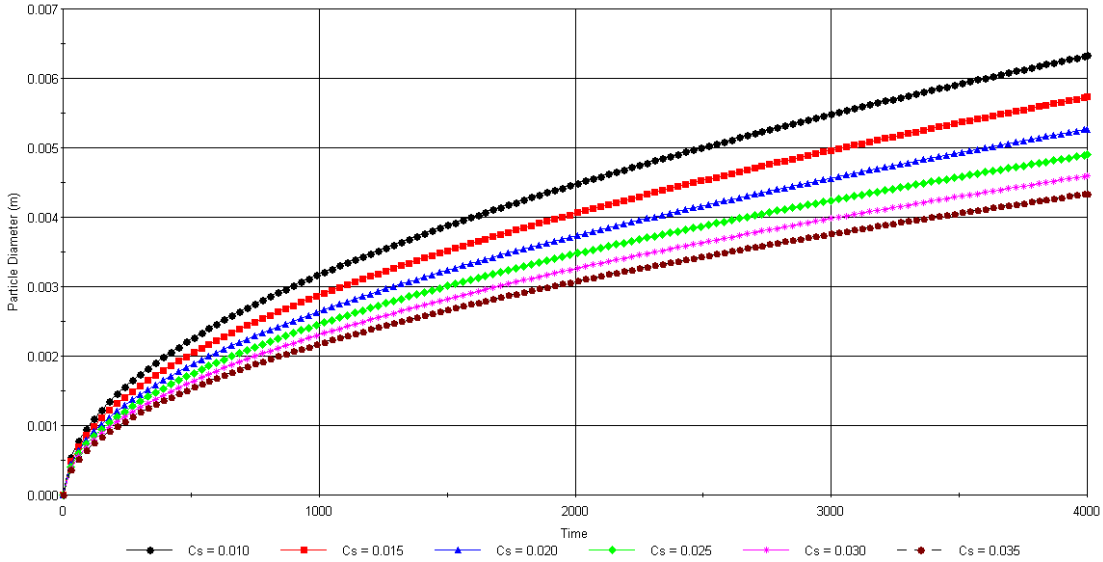

Fig. 17 Variation of crystal particle diameter versus time at different mass fraction of salt in brine feed

In theory, the growth rate of ice crystals is not always a straight-line, but a

parabolic curve, namely the growth rate of ice crystals slows down with the increase of salt concentration. Because of the salt ion being excluded from the crystal interface, the salt concentration of the interface is higher than that of the solution, thus the temperature of freezing point of the interface is below the freezing temperature of corresponding concentration of solution. Diffusion of mass transfer in the process of crystal growth is affected by the salt concentration of interface, and the freezing temperature difference of interface effects on the latent heat transfer released by ice crystals. Therefore, the higher the salt concentration is, the slower the heat transfer and mass transfer. The ice crystal growth rate decreases with the rising of salt concentration.

6. Conclusions

Here, a new idea of utilizing cold energy in LNG in freeze desalination is introduced, explained and modeled. As the LNG temperature is as low as -162 ^{o}C, the temperature difference would be too large for practical desalination if the cold energy were transmitted directly to the water. Therefore, an intermediate refrigerant is suggested to transfer the cold energy, while providing the most suitable seawater crystallization temperature.

The ice-making bucket of flake ice maker is selected as seawater crystallizer which has advantages of high heat transfer efficiency, continuous crystallization and removing ice without heat source.

The heat transfer around ice bucket of the freeze desalination process (Figure 5) is modeled using gPROMS. The behavior of the freeze desalination of the ice bucket on flake ice maker utilizing LNG cold energy may be predicted from the results obtained for the freezing section so far as nucleation and growth of solids present are concerned. Similarly, liquids behavior - their process parameters with respect to the refrigerant circulated around the freezing section and LNG flows through the heat exchanger - is predicted. The calculations show that the consumption of 1 kg equivalent of LNG cold energy can obtain about 2 kg of ice melt water.

From the energy consumption calculation presented, the LNG/FD hybrid process is found to cost power almost equal to zero.

Acknowledgements

The author is extremely grateful to the University of Bradford, as well as the 2013 Visiting Scholar Program of Fujian Province in China, which supported the

author (conferred the title of Honorary Visiting Academic) to research at the University of Bradford. This paper was financially supported by the Huang Huizhen Discipline Construction Foundation of Jimei University (ZC2012015) and Technology Project of Fujian Provincial Department of Education (JA12191). This work was also supported by the Technology Project of State Administration of Work Safety (201310180001).

References

[1] http://www.desalyearbook.com/market-profile/11-global-capacity (accessed 9th May 2014)

[2] Rizzuti, L, Ettouney HM, Cipollina, A solar desalination for the 21st century, NATO Security through Science Secries – C: Environmental Security, Springer, 2006.

[3] Rahman MS, Ahmed M, Chen XD, Freezing–melting process and desalination: review of present status and future prospects, Int. J. Nuclear Desalination 2 (2007) 253-264.

[4] Peng Wang, Tai-Shung Chung, A conceptual demonstration of freeze desalination-membrane distillation (FD-MD) hybrid desalination process utilizing liquefied natural gas (LNG) cold energy, Water Research 46 (2012) 4037-4052.

[5] Wen-sheng Cao, Xue-sheng Lu, Wen-sheng Lin, An-zhong Gu, Parameter comparison of two small-scale natural gas liquefaction processes in skid-mounted packages, Applied Thermal Engineering 26 (2006) 898-904

[6] LNG Journal November/December 2012.

[7] Xiao Dong Chen, Ping Chen, Kevin W. Free, A note on the two models of ice growth velocity in aqueous solutions derived from an irreversible thermodynamics analysis and the conventional heat and mass transfer theory, J. Food Eng. 31 (1997) 395-402.

[8] Signe Kjelstrup Ratkje, Ola Fleslandb, Modelling the freeze concentration process by irreversible thermodynamics, J. Food Eng. 25 (1995) 553-567.

[9] Y. Shirai, M. Wakisaka, O. Miyawaki, S. Sakashita, Effect on seed ice on formation of tube ice with high purity for a freeze wastewater treatment system with a bubble-flow circulator, Technical Note 33 (1999) 1325-1329.

[10] Ping Chen, Xiao Dong Chen, Kevin W. Free, An experimental study on the spatial uniformity of solute inclusion in ice formed from falling film flows on a sub-cooled surface, J. Food Eng. 39 (1999) 101-105.

[11] Minato Wakisaka, Yoshihito Shirai, Shigeru Sakashita, Ice crystallization in a pilot-scale freeze wastewater treatment system, Chemical Engineering and Processing 40 (2001) 201-208.

[12] Frank G.F. Qin, Xiao Dong Chen, Mohammed M. Farid, Growth kinetics of ice films spreading on a subcooled solid surface, Separation and Purification Technology 39 (2004)

109-121.
[13] J.D. Zhao, N. Liu, Y.M. Kang, Optimization of ice making period for ice storage system with flake ice maker, Energy and Buildings 40 (2008) 1623-1627.
[14] Warren Rice, David S.C. Chau, Freeze desalination using hydraulic refrigerant compressors, Desalination 109 (1997) 157-164.
[15] P.M. Williams, M. Ahmad, B.S. Connolly, Freeze desalination: An assessment of an ice maker machine for desalting brines, Desalination 308 (2013) 219-224.
[16] Ahmed A.A. Attia, New proposed system for freeze water desalination using auto reversed R-22 vapor compression heat pump, Desalination 254 (2010) 179-184.
[17] M.V. Rane, Y.S. Padiya, Heat pump operated freeze concentration system with tubular heat exchanger for seawater desalination, Energy for Sustainable Development 15 (2011) 184-191.
[18] Ryosuke Fujioka, Li Pang Wang, Gjergj Dodbiba, Toyohisa Fujita, Application of progressive freeze-concentration for desalination, Desalination 319 (2013) 33-37.
[19] Meibin Huang, Research of seawater desalination technology with LNG cold energy utilization, Master Dissertation of Shanghai Jiao Tong University, 2010.
[20] Wenquan Tao, Heat transmission science, Press of Northwestern Polytechnical University 2006.12.
[21] N. Akhtar, L. McGrath, P.D. Roberts, Dynamic modelling and partial simulation of a pilot scale column crystallizer, Desalination 28 (1979) 1-11.
[22] gPROMS. www.psenterprise.com.
[23] Gailing Bai, Present situation and development trend of natural gas liquefaction technology, Conference of natural gas purification, liquefaction, storage and utilization technology and equipments, 2011 China.

Table 2 Mole fractions of composition

Node	Phase	HFC-32	HFC-125	N_2	CH_4	C_2H_6	C_3H_8	iC_4H_{10}	nC_4H_{10}	iC_5H_{12}	nC_5H_{12}	C_6H_{14}	C_7H_{16}
1	Liquid	0.69762	0.30238	-	-	-	-	-	-	-	-	-	-
2	Vapour	0.69762	0.30238	-	-	-	-	-	-	-	-	-	
3	Liquid	0.69762	0.30238	-	-	-	-	-	-	-	-	-	
LNG	Liquid	-	-	0.00331	0.96994	0.01709	0.00481	0.00088	0.00204	0.00045	0.00107	0.00035	0.00006
NG	Vapour	-	-	0.00331	0.96994	0.01709	0.00481	0.00088	0.00204	0.00045	0.00107	0.00035	0.00006